Supplementary Figures:

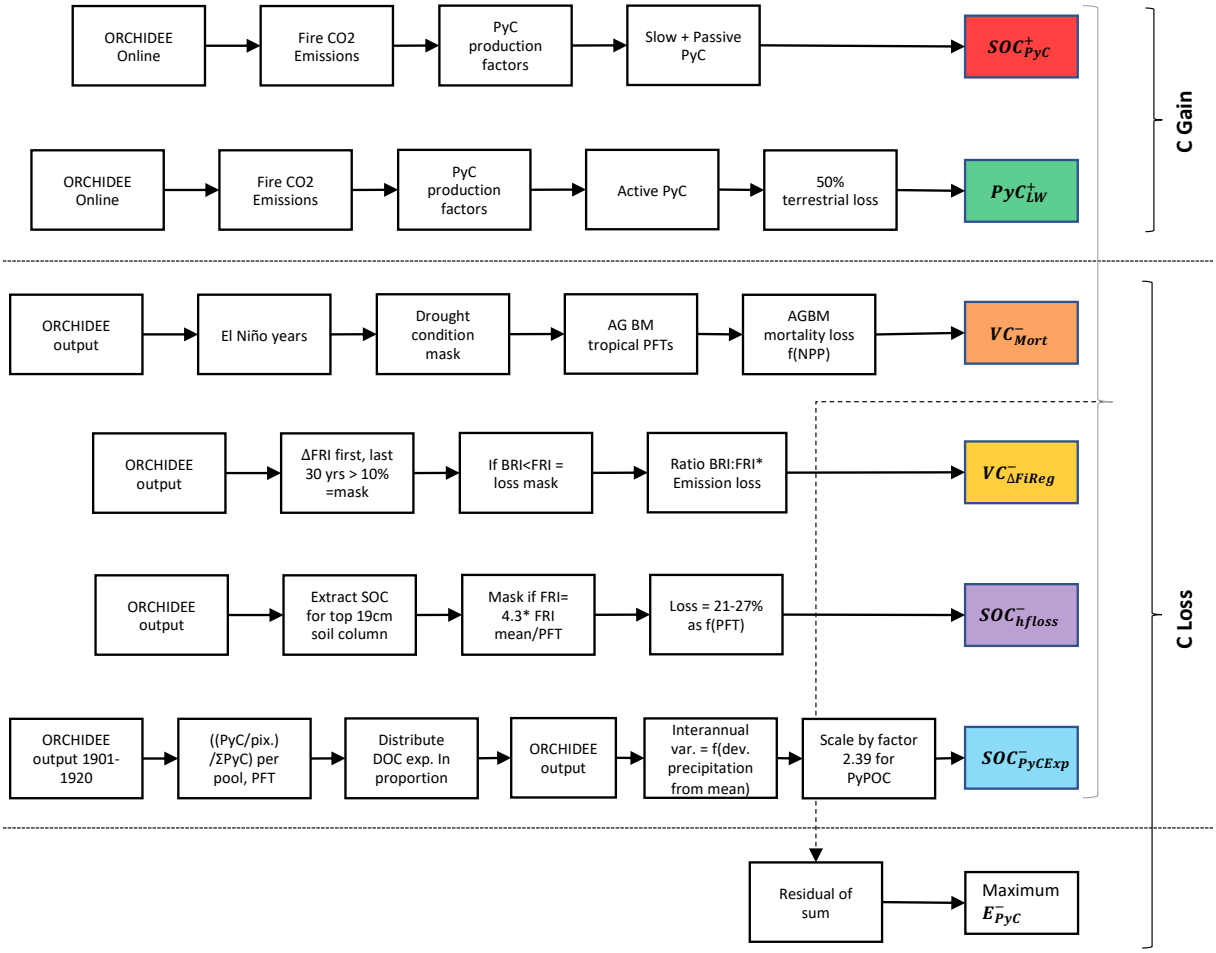

Figure S1: Simplified flow diagram illustrating the steps taken to estimate each of the terms in Equation 2. Refer to Methods for detail. AGBM refers to aboveground biomass, pix. pixel, and dev. deviation.

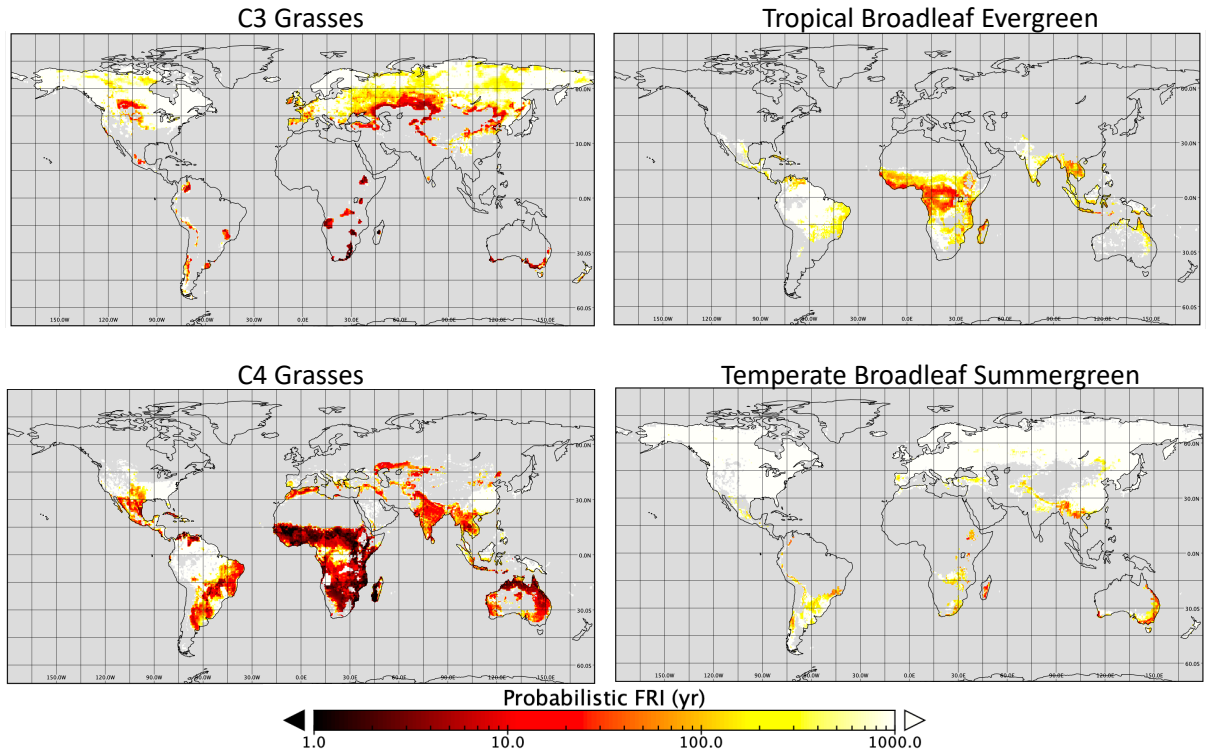

Figure S2: Probabilistic fire return interval (FRI -see *Methods*) for four illustrative PFTs, spatially averaged for each pixel and estimated over the course of the simulation.

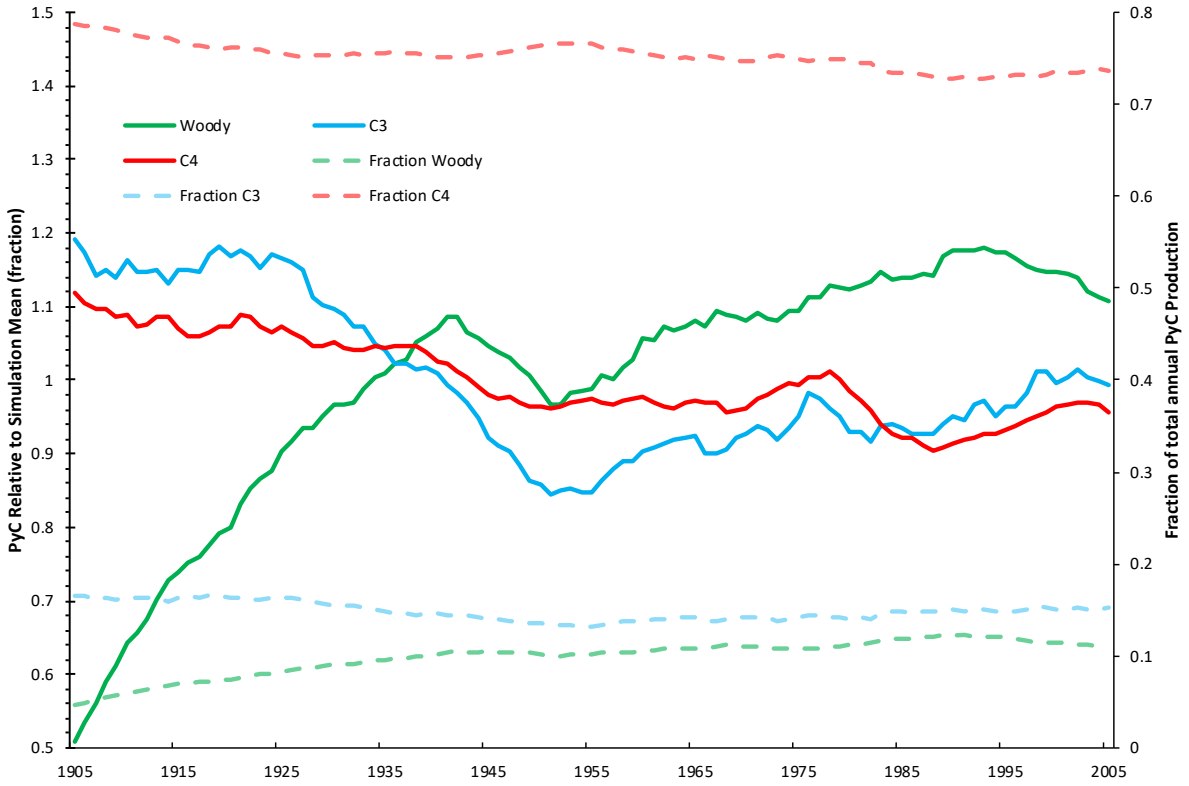

Figure S3: 10-year running average of globally summed woody, C3 and C4 grassland PyC (solid, primary y-axis) relative to the simulation mean value and (dashed, secondary y-axis) as a fraction of the summed annual PyC C production.

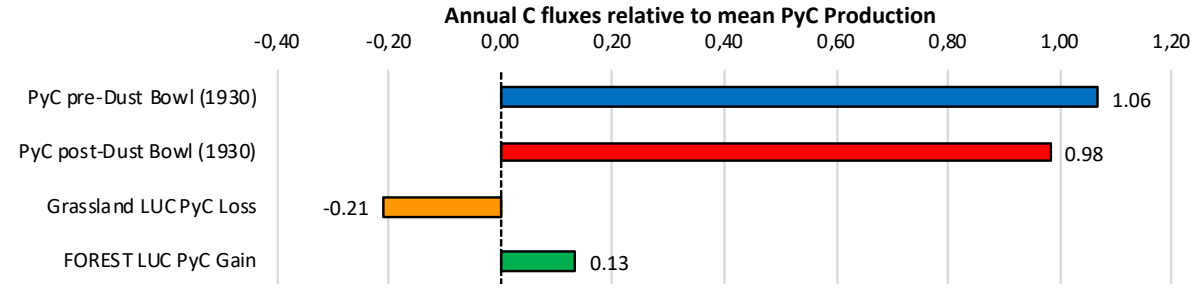

Figure S4: Pre- and Post- 1930 global PyC production relative to time-averaged PyC production, and estimated changes in PyC production between the periods (1901-1930) and 1931-2010) due to changes in land coverage (*VegArea*) by grassland and forest ((dPyC/dt)/(dVegArea/dt)), where LUC refers to land use change.

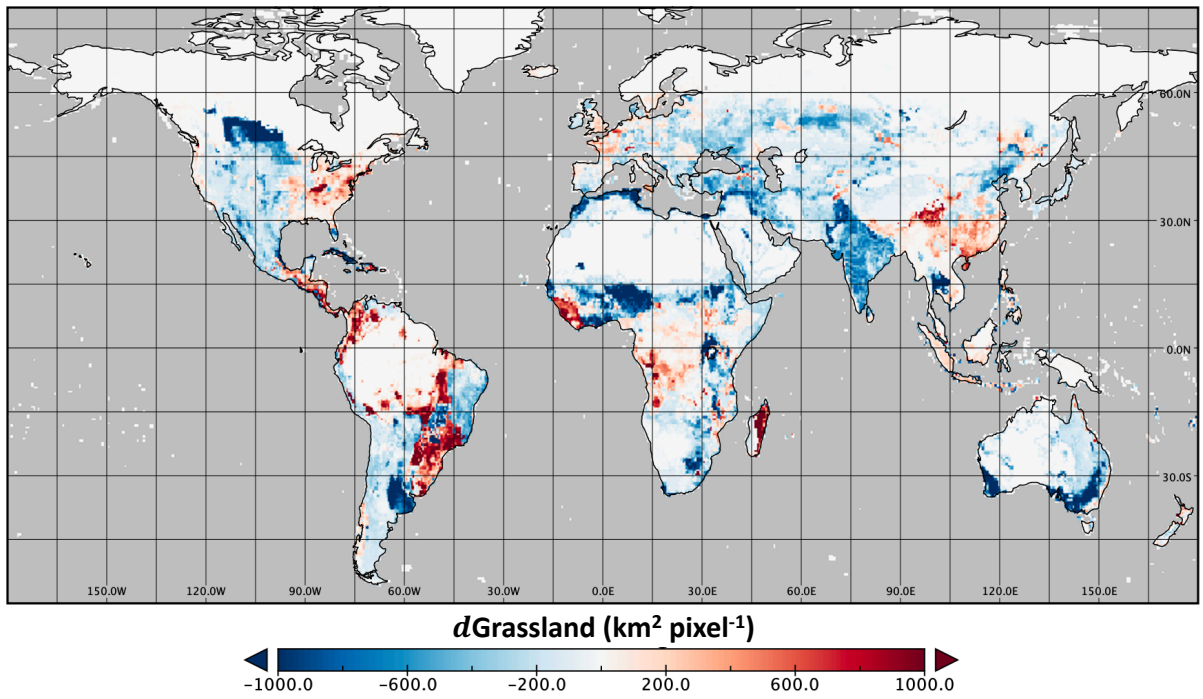

Figure S5: Change in grassland coverage between the average of the first and last decades of simulation.

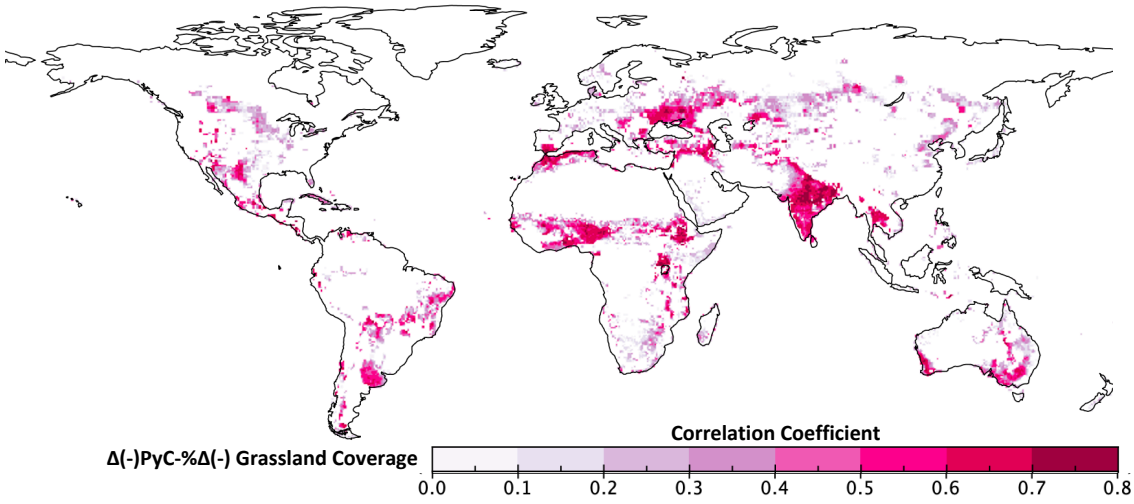

Figure S6: Per-timestep (n=1320) correlation coefficient between decreases in PyC production and decrease in grassland coverage, over the course of the simulation.

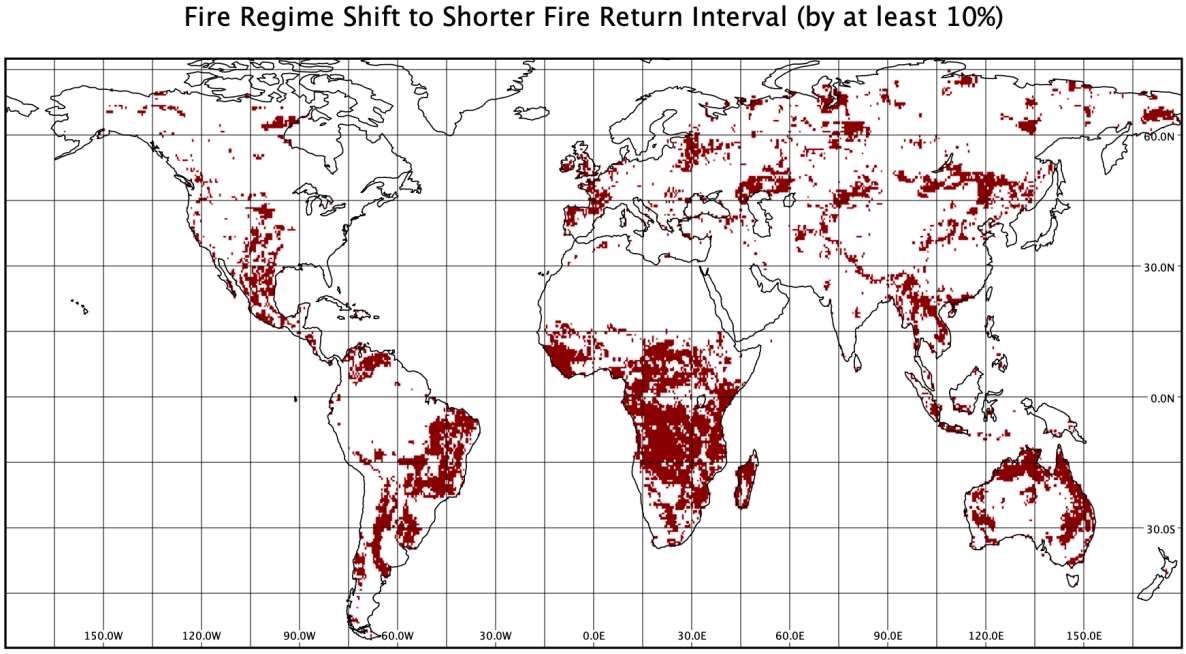

Figure S7: Areas where the estimated mean per pixel FRI decreased over the period 1901-2010 by a minimum of 10% on average, between the periods 1901-1930 and 1981-2010. Here change in per pixel FRI is calculated across PFTs weighted by the areal and fire coverage of each PFT on that pixel.

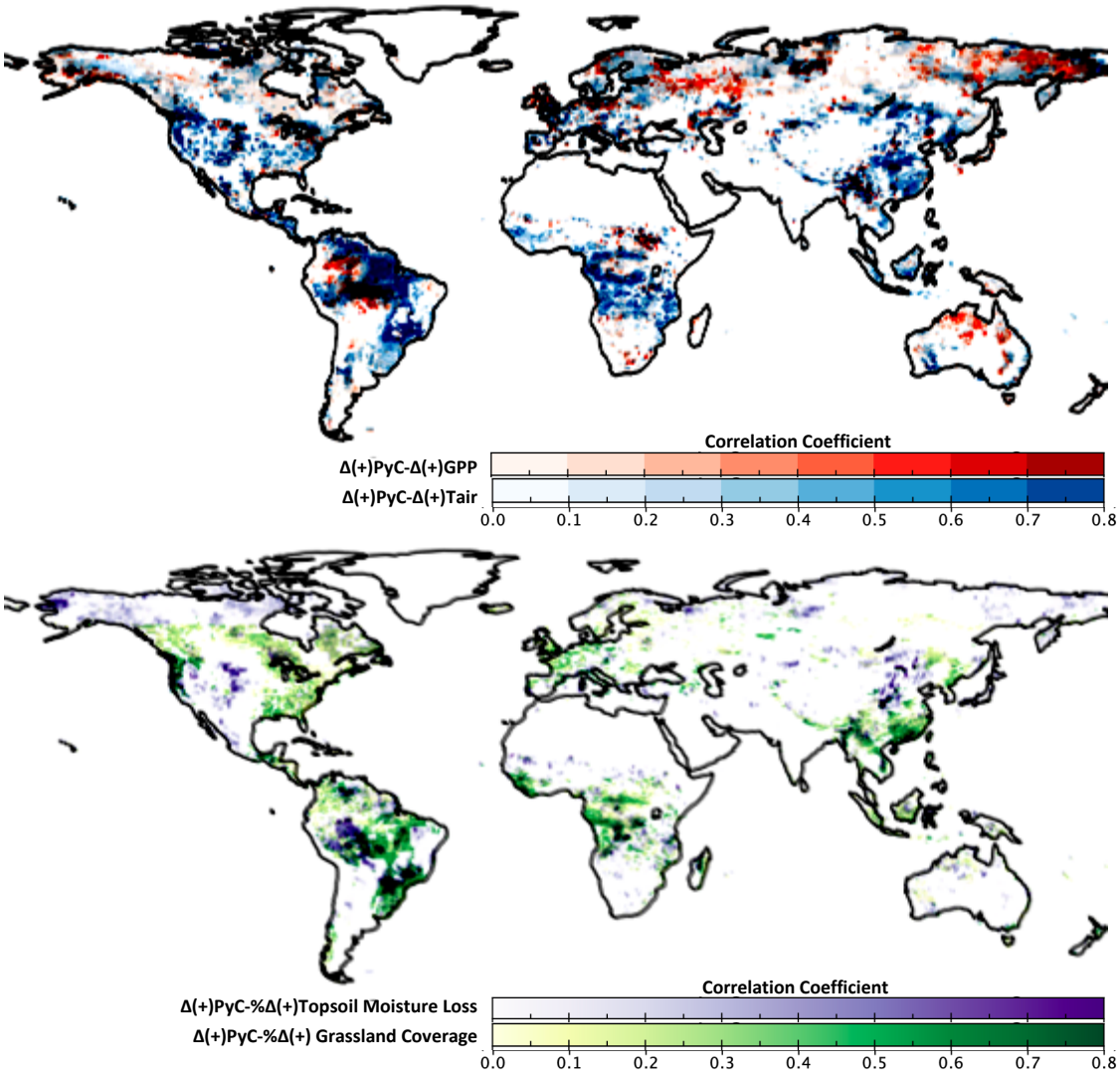

Figure S8: Per-timestep (n=1320) correlation coefficient between increases in PyC production and increases in GPP, air temperature, topsoil moisture loss and grassland coverage, over the course of the simulation.

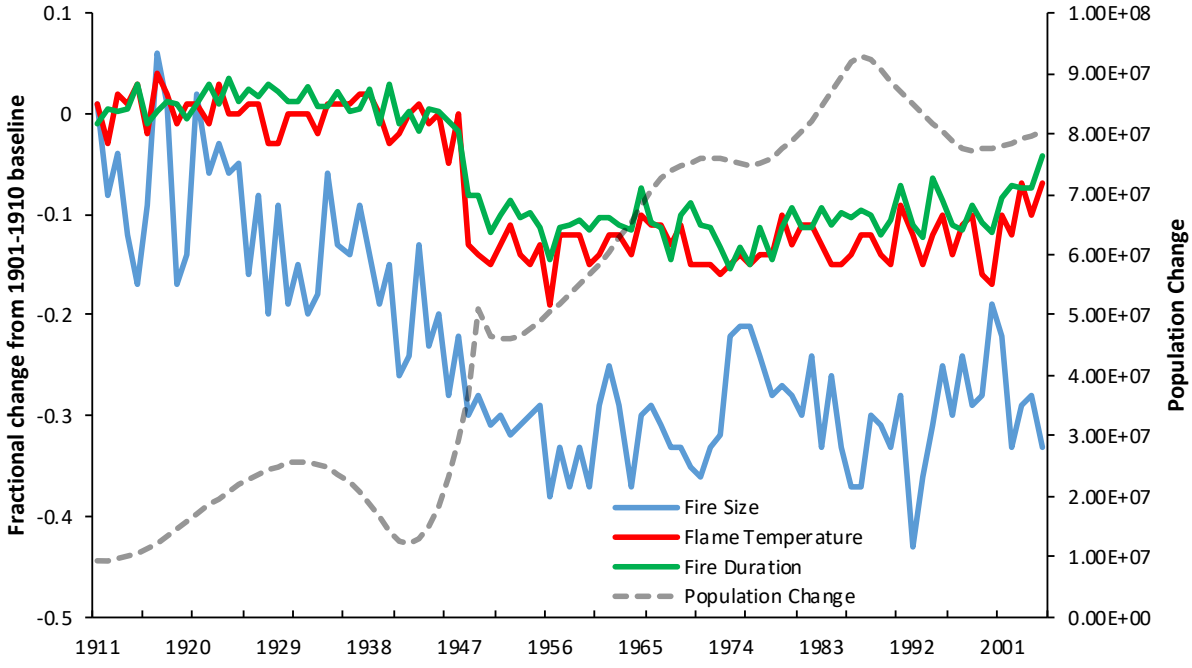

Figure S9: 20-year running mean of fractional changes in global spatially averaged fire characteristics (solid

lines, primary y-axis) and absolute changes in global human population (dashed line, secondary y-axis).

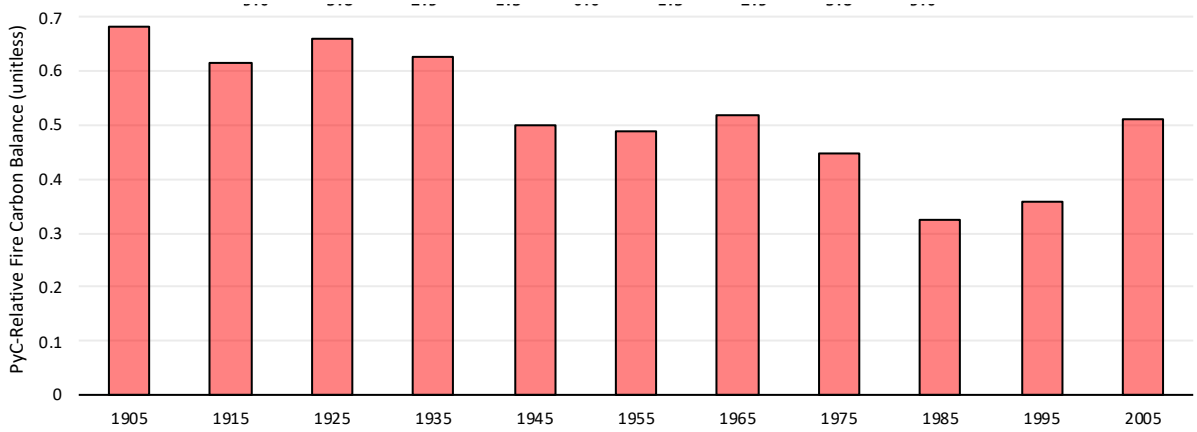

Figure S10: Globally-aggregated decadal mean fire C 'balance' as a fraction of decadal-mean PyC production (=1), over the simulation period.

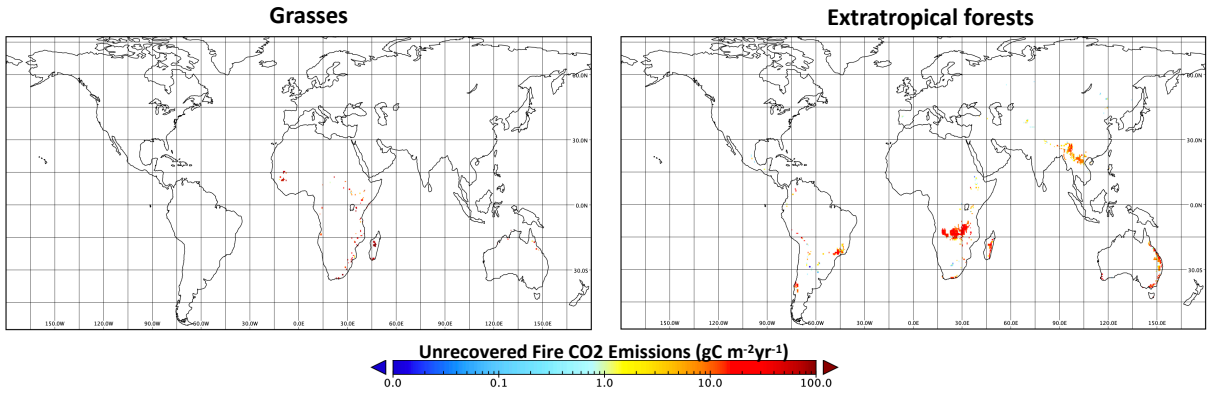

Figure S11: Time-averaged annual C losses (gC m^{-2} yr^{-1}) due to non-recovery of biome vegetation ($VC_{\Delta FiReg}$) to pre-disturbance state as the fire regime shifts and the FRI of a given biome shortens, split here into the sum of (left) grasslands, (right) forests.

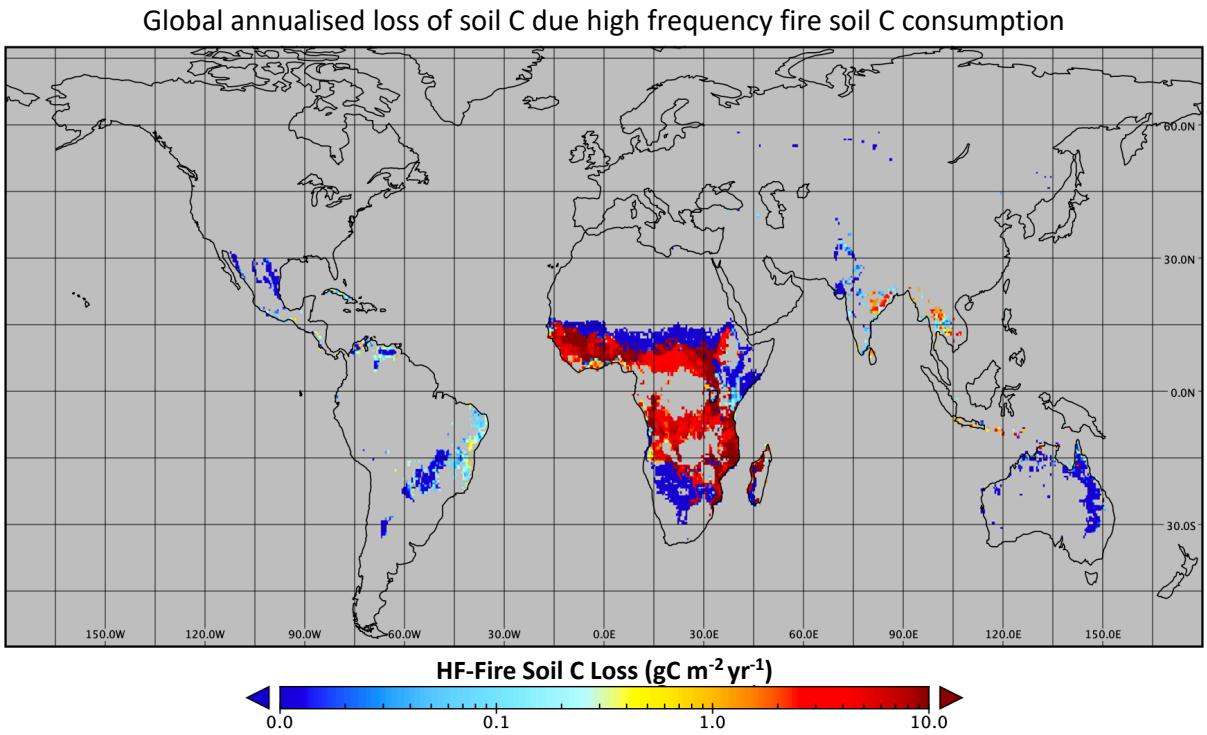

Figure S12: Time-averaged annual topsoil carbon loss (SOC^{-}_{hfloss}), in gC m^{-2} yr^{-1}, due to repeated (high frequency) fires summed over broad-leaf and grassland vegetation types, per ref. ([1]).

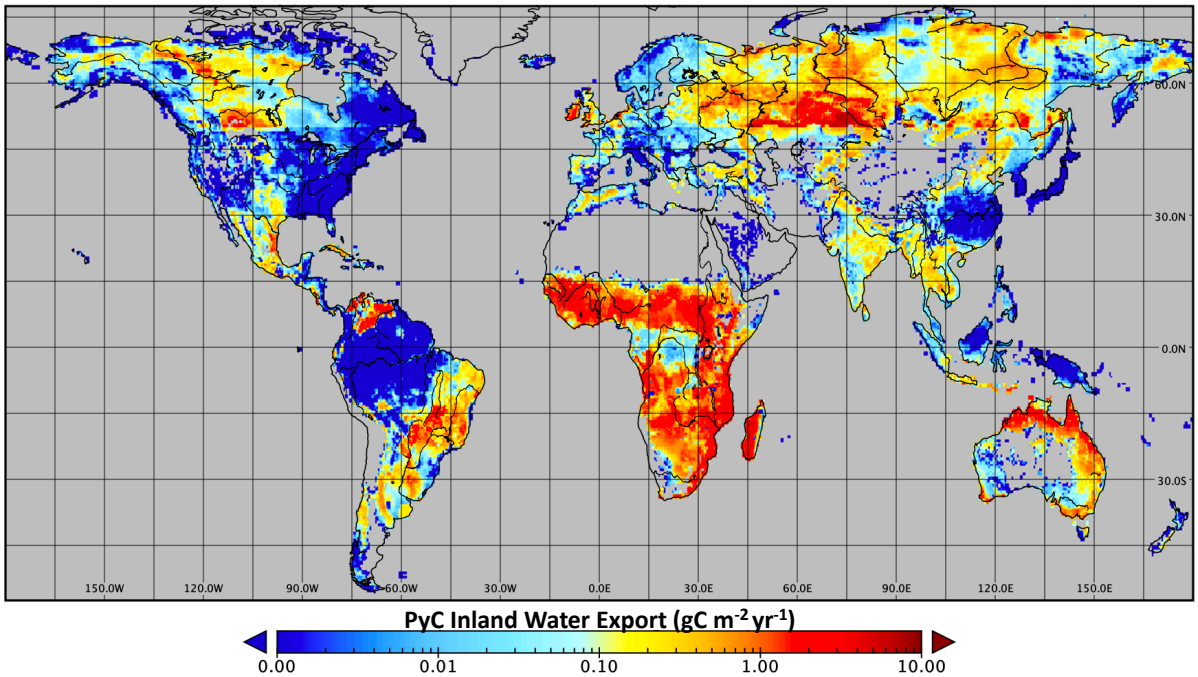

Figure S13: Estimated time averaged annual export of pyrogenic DOC and POC from the land surface to the inland aquatic network (SOC^{-}_{PyCExp}), emulated offline using data from refs. ([2,3]).

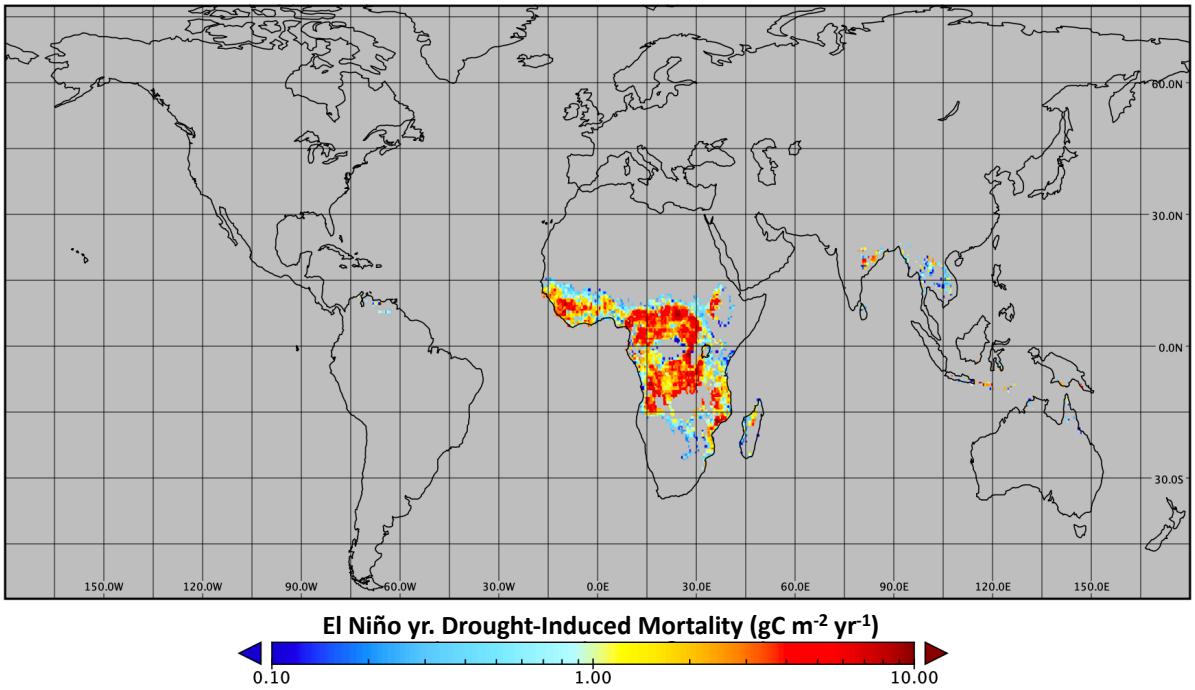

Figure S14: Estimated time averaged and annualised carbon loss from post-disturbance tropical vegetation mortality (VC^{-}_{Mort}) brought on by El Niño-induced drought fires (Methods).

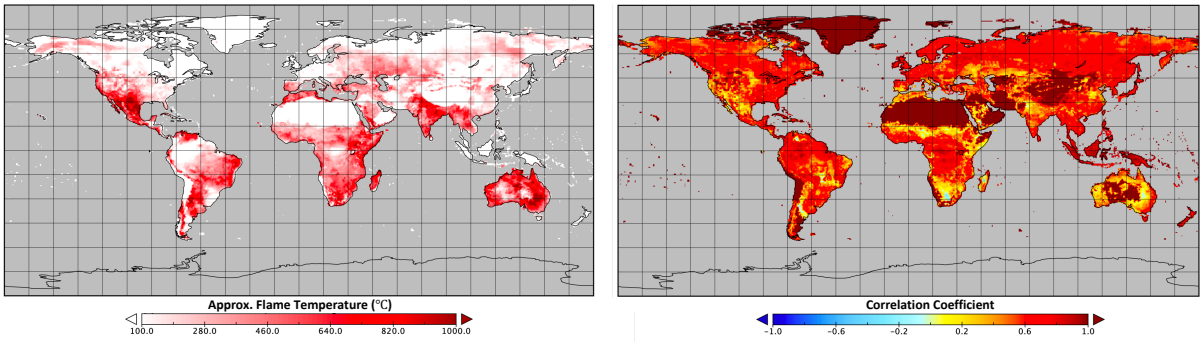

Figure S15: Simulation-mean (left) estimated pixel-average flame temperature of fire events, and (right) the correlation coefficient over the simulation period (n=1320) of PyC production with flame temperature.

Supplementary Tables:

	Aquatic Export (TgC yr^{-1})			
	Slow PyC DOC	Passive PyC DOC	Slow PyC DOC + POC	Passive PyC DOC + POC
Tropical broad-leaved evergreen	0.0243	0.0103	0.0581	0.0245
Tropical broad-leaved raingreen	0.0015	0.0047	0.0035	0.0113
Temperate needleleaf evergreen	0.0053	0.0006	0.0128	0.0015
Temperate broad-leaved evergreen	0.1342	0.0111	0.3205	0.0266
Temperate broad-leaved summergreen	0.0092	0.0011	0.0219	0.0026
Boreal needleleaf evergreen	0.0440	0.0070	0.1052	0.0167
Boreal broad-leaved summergreen	0.0471	0.0123	0.1124	0.0295
Boreal needleleaf summergreen	0.0058	0.0030	0.0139	0.0070
C3 Grass Temperate	0.1978	1.5041	0.4726	3.5931
C4 Grass	1.6280	10.7431	3.8892	25.6640
C3 Grass Boreal	0.5133	3.2497	1.2262	7.7632
C3 Sum	0.7111	4.7538	1.6988	11.3563
	SUM	18.158		43.376

Table S: Model-derived estimates of pyrogenic DOC (two left columns) and DOC+POC (two right columns) outflow, via the two pools of PyC represented here, from the terrestrial landmass originating from each of the 10 non-agricultural vegetation types in the model. The 3 global biomes identified in ref. () are represented in colour (green=tropical; orange=temperate; blue=boreal).

Vegetation Type	Max. Flame Temp (C)	Mean Flame Temp (C)	Index
Tropical broad-leaved evergreen	1089	286	0.57
Tropical broad-leaved raingreen	1730	420	0.84
Temperate needleleaf evergreen	1183	337	0.67
Temperate broad-leaved evergreen	1302	422	0.84
Temperate broad-leaved summergreen	1559	453	0.91
Boreal needleleaf evergreen	803	194	0.39
Boreal broad-leaved summergreen	639	175	0.35
Boreal needleleaf summergreen	1035	195	0.39
C3 Grass	1120	335	0.67
C4 Grass	1445	501	1.00

Table S: Approximate maximum (left) and mean (centre) annual flame temperatures for each PFT, averaged over the length of the simulation, and normalised (right) to the maximum value (C4 grass =1). Temperature is estimated from flame intensity outputs using the equation $Q = \mathcal{E} * k * T^4$, where Q is flame power, $\mathcal{E}$ the emissivity of the combusting material (here assumed 0.9 for wood), k the Boltzmann constant and T flame temperature.

Supplementary Discussion

Supplementary Text S1: Considerations regarding the partial fire carbon balance and MRT

The 'fire C balance' as constructed here is the partial (excluding PyC mineralisation emissions) net flux of carbon post-fire with respect to the terrestrial biosphere, not with respect to the atmosphere. This is an important distinction because what is lost from the land surface, for example aquatic export from the soil to rivers, may not necessarily be subsequently emitted to the atmosphere. To be sure, once suspended in overland water flow potentially large amounts of dissolved PyC are liable to rapid in-stream photo-oxidation[4–6], amounting (e.g.) to between 23-40% of annually mobilised Py-DOC in Brazil's Paraíba Do Sul river[6]. On the other hand, in their movement towards marine sediments particulate PyC is thought to be highly resistant to in-transit degradation, with a seafloor depositional flux of 17-37 TgC yr^{-1}. The bulk fate of this seafloor Py-POC is unknown, but hypoxic or effectively anoxic conditions coupled with low light and temperature levels in that environment suggest considerably lower rates of mineralisation than at the land-atmosphere interface. This essentially conservative behaviour[7] entails the potential for atmospheric sequestration of PyC at geological timescales (limited by uplift, subduction, subsea tectonic spreading).

There remains at present insufficient empirical data and process understanding to partition the quantities and rates of PyC oxidation/sequestration once exported from the terrestrial landmass. For these reasons, in this study we can only consider the PyC balance with respect to the global land surface, a formulation which necessarily underestimates the positive (sequestered PyC) terms of the balance (Eq. 2) if they were considered with respect to atmospheric flux. The upshot is that the 'real' net positive C balance of fires globally may be substantially larger than that estimated here (or potential PyC mineralisation rates substantially higher).

Similar considerations feed into the concept of *in situ* PyC residence time used here. Once produced, PyC may be oxidised, incorporated vertically into the soil column or transported laterally over the landscape. However, the theoretical underpinnings of PyC oxidation and the factors modulating it are complicated by its persistence and relatively mobile nature. Estimates of PyC MRT and the effects of fire intensity and duration on it are estimated in laboratory incubation experiments and mineralisation rates/MRTs calculated by extrapolation from a narrow time sample over hundreds to thousands of years. The definition of residence time itself differs between studies, with most benchmarked by oxidation of PyC to CO_2, and few others by their export out of the incubation chamber (either by oxidation or by dissolved/micro-particulate transport)[8,9]. This means that literature-derived PyC MRT and the conditions modulating it are based on two potential pathways: flux to the atmosphere, and [conservative] transport out of a particular soil pedon. For consistency therefore, we expand the traditional notion of MRT to a dual pathway concept (here, *in situ* MRT), in a manner analogous to the definition of fire C balance used herein.

Supplementary Text S2: Note on PyC derived from 1hr fuel

Of the PyC derived from the four fuel classes, PyC_{LW}^{+} which is derived from 1-hour fuels is excluded from entering the two Py-SOC pools and is assumed in the analysis to be 50% mineralised or exported within the first year of its production. In doing so we assume that because 1hr fuels are derived from small initial pieces of vegetation biomass (since fuel class number is a f(time to remove moisture from fuel = f(volume or diameter of fuel)) comprising

in reality twigs, leaves and the like, particle sizes of the PyC_{1hr} product are likewise very small to begin with. This would confer higher mass-normalised surface area relative to larger PyC particles, making the relatively 'labile' component more readily available to microbial uptake and consumption. Likewise, small particles are by definition more readily mobilised both vertically and laterally, with large amounts potentially flowing out into the inland water network or groundwater where they may be may be emitted by photooxidation or redeposited in intermediary 'holding' sites for thousands of years[2]. Reflecting the uncertainty in either of these potential fates, we make the simplifying assumption that half of this material is lost as either SOC^{-}_{PyCExp} or E^{-}_{PyC}, and are thus implicitly included in these terms in the analysis.

Supplementary Text S3: On estimated El Niño-induced drought and post-fire mortality loss

We estimate very little drought induced mortality from the Amazon region (a small portion along its northern edge, Fig. S6), despite the parameters used to derive the calculation of this variable coming from empirically derived Amazonian data. This may be due to either an overly conservative definition of drought (a statistical assumption), extremely low historical fire return intervals in the Amazon as simulated by SPITFIRE (BRI<FRI, meaning we assume eventual biospheric recovery), or due to our lack of simulated deforestation fires in this model configuration.

Supplementary Text S4: Note on estimating FRI

Estimating per-Plant Functional Type (PFT) FRI from ORCHIDEE is complicated by the fact that FRI is an area-specific quantity (the average time it takes for a fire to return to a given parcel of land), while the simulation of area burned is not a PFT-specific quantity (the area that is burned annually is simply a fraction of a pixel, not denominated by specific vegetation types). On the other hand, per pixel fire emissions are PFT-specific. Thus, working on the assumption that fractional emissions from each PFT are proportional to the fraction of burned area of that PFT, a probabilistic FRI was calculated. The burned fraction (BF) of each pixel per timestep is extracted and converted to area burned per pixel and timestep (BA). The burned area of each PFT is unknown, and must be estimated probabilistically based on PFT-specific CO2 emissions.

Supplementary Text S5: Considerations in BRI parameter estimates

i

The maximum fractional variation of PFT and pixel -specific BRI from the central value (the Beta term in Eq. 6) is relatively low for grasses, reflecting an expectation that PFT-specific BRI is likely to vary less than forests due to the already low BRI value (that grasses are unlikely to recover within e.g. 3 months) and the fact that grasses are fire-adapted (they will recover within <4yrs). The forest Beta term reflects the huge variation in recovery between species, ecosystems, fire regimes, landscapes and biomes which our simple NPP-variant methodology will necessarily fail to properly capture. Nonetheless, we believe that at the first order, these remain sufficient to approach the loss terms discussed in the following sections.

For tropical BRI, given extremely poor data constraints with respect to tropical forest recovery to fire-specific disturbance, and the fact that tropical forest FRI exceeds the simulation length for almost all pixels, we assume that vegetation non-recovery due to FRI<BRI is globally zero. But in attempting to estimate recovery from forest dieback plus C-loss due to forest fire emissions in tropical forests, one must estimate a recovery time for the combined loss from

both immediate vegetation combustion and longer-term post fire mortality. For this we opted for a slightly different approach. Based on existing available data[10], mean post-fire aboveground biomass carbon mortality losses from El Niño drought induced fires in the Amazon is ~24.7%, with mortality taking place over a 30 year period, which is non-saturating over that time (although losses become very weak towards its end)[10,11]. Assuming this loss is linear gives -0.83% yr^{-1}. Since the loss in non-saturating, we assume that losses and gains are zero over yrs. 31-40 of the recovery period, following which they begin to increase at a rate of 1.2% yr^{-1} based on post-fire recovery estimates in ref. ([12]). This gives a central tropical forest post-fire recovery time of 121.3 years (100/1.2=81.3 yrs + 40 years of losses), which varies by ±50% as a function of NPP relative to $\overline{NPPm_{Global}^{PFT}}$ for tropical PFTs.

The uncertainty range for $VC_{\Delta FiReg}$ is based on parameter uncertainty involving the central BRI value. Thus we assume that C3 and C4 can have a max/min central BRI value of (3,2) and (2/1) years, respectively. For extratropical forests we use the standard error of the empirical literature review to arrive at forest central BRI max/min values of 170/96 years.

Supplementary Text S6: Note on implied PyC MRT as a function of fire intensity

Our results show that fires burning over tropical C4 grassland regions sustain some of the highest flame intensities amongst vegetation types (Table S2), forest crown fires notwithstanding (as they are only implicitly represented, see main text and ref. ([13])), implying, given current understanding of the effects of fire characteristics on the PyC product, a relatively higher mean residence time of PyC originating from C4 grasses. This is in contradiction to the initial hypothesis and Figure 1, which postulates lower flame intensities and hence MRT for grasses, on the basis that short fire return intervals result in lower pre-fire biomass accumulation and less fuel to support high intensity fires. Conversely, modelled C3 grassland fires exhibit flame intensities lower than at least half of other vegetation types (Table S2). Even in the absence of crown fire representation, maximum flame temperatures for isolated fire events are higher for certain woody vegetation types than either C3 or C4 grasslands, a result which holds across latitudes. That ORCHIDEE fire simulations result in higher flame intensities for C4 grasses (while C3 grasses are subject to some of the lowest flame intensities) is, we believe, the result of three factors: (a) Grass species in the tropics by definition receive higher rates of incident solar radiation, such that tropical grasses are subject to higher NPP rates on average than grasses in temperate and boreal regions, allowing for the production of substantially larger amounts of potential fuel. (b) Tropical grasses tend to exist in arid and semi-arid regions where forests would otherwise dominate, such that potential fuel is liable to substantial or near-total desiccation, facilitating rapid high intensity combustion, in comparison to temperate grasses. (c) Biomass allocation to belowground organs (up to 80%) in tropical grasses allows for rapid post-fire recovery and hence sustained fuel loading for high intensity fires to recur.

Supplementary Text S7: Back-envelope estimate of PyC MRT

The back-envelope estimates of minimum PyC MRT are made on the basis of a mix of existing stock and flow estimates, as well as the estimated maximum mineralisation rate found in this study. This is calculated using the maximum PyC mineralisation rate (E_{PyC}^{-}), the estimated fraction of PyC in global SOC ($fPyC_{SOC}$), the estimated annual mineralisation of bulk SOC (E_{SOC}) and the estimated bulk mean MRT of SOC globally (MRT_{SOC}). PyC MRT (MRT_{PyC}) is estimated by:

$$\boldsymbol{MRT_{PyC} = (fPyC_{SOC}/(\frac{E_{PyC}^{-}}{E_{SOC}})) * MRT_{SOC}} \qquad \textbf{(Eq. S1)}$$

References

1. Pellegrini, A. F. A. *et al.* Fire frequency drives decadal changes in soil carbon and nitrogen and ecosystem productivity. *Nature* (2018). doi:10.1038/nature24668
2. Coppola, A. I. *et al.* Global-scale evidence for the refractory nature of riverine black carbon. *Nat. Geosci.* (2018). doi:10.1038/s41561-018-0159-8
3. Jones, M. W. *et al.* Fires prime terrestrial organic carbon for riverine export to the global oceans. *Nat. Commun.* (2020). doi:10.1038/s41467-020-16576-z
4. Spencer, R. G. M. *et al.* Photochemical degradation of dissolved organic matter and dissolved lignin phenols from the Congo River. *J. Geophys. Res. Biogeosciences* (2009). doi:10.1029/2009JG000968
5. Stubbins, A. *et al.* Relating carbon monoxide photoproduction to dissolved organic matter functionality. *Environ. Sci. Technol.* (2008). doi:10.1021/es703014q
6. Marques, J. S. J. *et al.* Dissolved black carbon in the headwaters-to-ocean continuum of Paraíba do Sul River, Brazil. *Front. Earth Sci.* (2017). doi:10.3389/feart.2017.00011
7. Salvadó, J. A., Bröder, L., Andersson, A., Semiletov, I. P. & Gustafsson, Ö. Release of Black Carbon From Thawing Permafrost Estimated by Sequestration Fluxes in the East Siberian Arctic Shelf Recipient. *Global Biogeochem. Cycles* (2017). doi:10.1002/2017GB005693
8. Lutfalla, S. *et al.* Pyrogenic carbon lacks long-term persistence in temperate arable soils. *Front. Earth Sci.* (2017). doi:10.3389/feart.2017.00096
9. Maestrini, B., Herrmann, A. M., Nannipieri, P., Schmidt, M. W. I. & Abiven, S. Ryegrass-derived pyrogenic organic matter changes organic carbon and nitrogen mineralization in a temperate forest soil. *Soil Biol. Biochem.* (2014). doi:10.1016/j.soilbio.2013.11.013
10. Silva, C. V. J. *et al.* Drought-induced Amazonian wildfires instigate a decadal-scale disruption of forest carbon dynamics. *Philos. Trans. R. Soc. B Biol. Sci.* (2018). doi:10.1098/rstb.2018.0043
11. Brando, P. M. *et al.* Prolonged tropical forest degradation due to compounding disturbances: Implications for CO2 and H2O fluxes. *Glob. Chang. Biol.* (2019). doi:10.1111/gcb.14659
12. Lennox, G. D. *et al.* Second rate or a second chance? Assessing biomass and biodiversity recovery in regenerating Amazonian forests. *Glob. Chang. Biol.* (2018). doi:10.1111/gcb.14443
13. Yue, C. *et al.* Modelling the role of fires in the terrestrial carbon balance by incorporating SPITFIRE into the global vegetation model ORCHIDEE - Part 1: Simulating historical global burned area and fire regimes. *Geosci. Model Dev.* (2014). doi:10.5194/gmd-7-2747-2014